Geomechanics and Engineering, *Vol. 12, No. 6 (2017) 1003-1020*
DOI: https://doi.org/10.12989/gae.2017.12.6.1003

Estimation of groundwater inflow into an underground oil storage facility in granite

Zhechao Wang [*1,2], Sangki Kwon [3a], Liping Qiao [1b], Liping Bi [4c] and Liyuan Yu [2d]

[1] *Key Laboratory of Ministry of Education on Safe Mining of Deep Metal Mines, Northeastern University, Shenyang, Liaoning, 110004, China*
[2] *State Key Laboratory for Geomechanics and Deep Underground Engineering, China University of Mining & Technology, Xuzhou, Jiangshu, 221008, China*
[3] *Department of Energy Resources Engineering, Inha University, Chung-Hak Dong, Yeun-Su Ku, Incheon, 402751, Korea*
[4] *Geotechnical and Structural Engineering Research Center, Shandong University, Jinan, Shandong, 250061, China*

(*Received July 01, 2016, Revised December 20, 2016, Accepted January 25, 2017*)

Abstract. Estimation of groundwater inflow into underground opening is of critical importance for the design and construction of underground structures. Groundwater inflow into a pilot underground storage facility in China was estimated using analytical equations, numerical modeling and field measurement. The applicability of analytical and numerical methods was examined by comparing the estimated and measured results. Field geological investigation indicated that in local scale the high groundwater inflows are associated with the appearance of open joints, fractured zone or dykes induced by shear and/or tensile tectonic stresses. It was found that 8 groundwater inflow spots with high inflow rates account for about 82% of the total rate for the 9 caverns. On the prediction of the magnitude of groundwater inflow rate, it was found that could both (Finite Element Method) FEM and (Discrete Element Method) DEM perform better than analytical equations, due to the fact that in analytical equations simplified assumptions were adopted. However, on the prediction of the spatial distribution estimation of groundwater inflow, both analytical and numerical methods failed to predict at the present state. Nevertheless, numerical simulations would prevail over analytical methods to predict the distribution if more details in the simulations were taken into consideration.

Keywords: groundwater inflow; rock caverns; numerical modeling, analytical solution; field measurement; heterogeneity

1. Introduction

Reliable estimation of groundwater inflow into underground openings is of critical importance for the design and construction of underground facilities in a rock mass. The accuracy of the estimation relies on the characterization of rock mass, the mechanism for groundwater flow in rock

*Corresponding author, Ph.D., Professor, E-mail: wanz@sdu.edu.cn
[a] Ph.D., Professor, E-mail: kwonsk@inha.ac.kr
[b] Professor, E-mail: qiaolp@sdu.edu.cn
c M.Sc. Student, E-mail: 136194411@qq.com
d Ph.D., Associate Professor, E-mail: yuliyuan@cumt.edu.cn

http://www.techno-press.org/?journal=gae&subpage=7 ISSN: 2005-307X (Print), 2092-6219 (Online)

mass and the initial and/or boundary conditions used for the estimation. In literature, groundwater inflow is usually estimated using analytical equations (e.g., Harr 1962, El Tani 2003, Kolymbas and Wagner 2007, Perrochet and Dematteis 2007, Park *et al*. 2008, Moon and Fernandez 2010, Marechal *et al*. 2014), numerical modeling (e.g., Li *et al*. 2014, Mas Ivars 2006, Fernandez and Moon 2010b, Molinero *et al*. 2002, Coli *et al*. 2008), or field measurement (e.g., Cesano *et al*. 2000, Zarei *et al*. 2011).

For analytical equations, the rock mass was usually assumed to be isotropic and homogeneous and the groundwater flow through rock mass was assumed to be in steady state, while simple boundary conditions, i.e., constant groundwater table above openings (Harr 1962, El Tani 2003, Kolymbas and Wagner 2007, Park *et al*. 2008) and zero water pressure at tunnel periphery (Harr 1962, El Tani 2003, Moon and Fernandez 2010) were used for the derivation of the equations. It was reported that the estimated rate was usually much higher than that in field observation (Moon and Fernandez 2010, Fenandez and Moon 2010a). In recent years, efforts have been devoted to derive analytical equations for the estimation of groundwater inflow under complex boundary conditions, such as, constant water head at tunnel periphery (Kolymbas and Wagner 2007, Park *et al*. 2008), varying groundwater table (Moon and Fernandez 2010) and heterogeneous formation (Perrochet and Dematteis 2007, Marechal *et al*. 2014).

Numerical modeling has become one of the most powerful tools for the estimation of groundwater inflow into underground openings, especially under complex situations. As a Discontinuous, Anisotropic, Inhomogeneous and Non-Elastic (DIANE) medium, the permeable properties of rock mass depend on the geometrical and geotechnical properties of fracture networks in rock mass (Harrison and Hudson 2000, Jing 2003, Liu *et al*. 2015, 2016a, b, c). The methods to evaluate the permeable properties of rock mass are of critical importance in both continuous and discontinuous numerical modeling (Cesano *et al*. 2003, Coli *et al*. 2008). Moreover, the effect of hydro-mechanical coupling was considered in a more general situation (Mas Ivars 2016, Fernandez and Moon 2010a, b, Wang *et al*. 2015a).

Field measurement would provide good estimations on the groundwater inflow into underground openings. However, the reports on field studies are few in literature due to the fact that field measurements are usually time and labor consuming, especially for large scale underground facilities. Among the field studies, Cesano *et al*. (2000) performed a statistical analysis on the parameters regulating groundwater inflows into tunnels. Zarei *et al*. (2011) investigated the role of geological features on high local groundwater inflow into a rock tunnel. Perello *et al*. (2014) measured the time-dependent groundwater inflow rates into a pilot tunnel in granitic massifs during and after tunnel excavation.

In China, a national crude oil storage project is undergoing. Underground caverns with water curtain system are being used for the project. For the design and construction of such underground oil storage facilities, the estimation on the groundwater inflow is one of the critical issues. The magnitude and spatial distribution of groundwater inflow would take effect on the capacity of pumping system and the operation cost of the facility. In this study, groundwater flow into the pilot underground storage facility was estimated using analytical equations, numerical modeling and field measurement. The measured and predicted magnitude and spatial distribution of groundwater flow rate were compared. The implications from the comparison on the applicability of the prediction methods were presented. A series of field permeability tests was performed to obtain the permeability coefficients of rock mass. Analytical equations were used to predict the groundwater flow rate of the facility. Finite Element Method (FEM) and Discrete Element Method (DEM) were employed to predict the magnitude and spatial distribution of groundwater inflow into the facility.

The groundwater inflow rates into the different caverns and the spatial distribution of leakage spots in the project area were measured in terms of the types of groundwater leakage spots. The nonuniformity of spatial distribution of groundwater inflow was identified. The geological conditions for high groundwater inflow spots were investigated. The applicability of numerical modeling and the discrete nature of spatial distribution of groundwater flow rate for jointed rock mass were discussed using the comparison of the predicted results with measured results.

2. Site description

2.1 General

The underground facility is composed of three distinct groups, storage caverns, access tunnels and water curtain tunnels. All cross sections are of horseshoe shape. That is, level floor and semi-circular roof. The width of the facility is approximately 500 m.

The 9 storage caverns are parallel, aligned in the direction N50°W and designed to operate as 3 groups A (#1, 2, 3), B (#4, 5, 6) and C (#7, 8, 9). Each group is used to store crude oil from a particular source. The storage caverns have dimensions of width 20 m, height 30 m and length 500 ~ 700 m. The floor level is EL (-50 m). EL denotes elevation in this paper. The access tunnels are 7.5 m wide and 8.5 m high and their elevation is EL (+70 m) at the entry level and EL (-50 m) at the floor level of storage caverns. See Fig. 1 for their locations in relation to the storage caverns. The water curtain tunnels are 4.5 m wide and 5.5 m high and floor level is EL (+5 m) that is 25 m above the storage caverns. Five water curtain tunnels across the nine storage caverns were placed over the storage facility. On the sidewall of water curtain tunnels, water curtain boreholes of a diameter of 180 mm were drilled with an initial spacing of 10 m. The water curtain tunnels and boreholes will provide supply of groundwater for the storage in order to maintain the containment of the facility (Wang *et al*. 2015b, c).

The excavation of the tunnels and caverns was by the drill and blast method. Excavation of storage caverns was in four lifts, gallery and benches 1 to 3 of heights 7.5, 10, 10, 2.5 m, respectively. Support for the caverns is by a combination of rock bolts and shotcrete. The system used was determined by past experience obtained in the construction of caverns in local hydro-power industry. The excavated section was supported before the working face advances 60 m. Rock bolts with a diameter of 28 mm were inserted in pre-drilled holes and grouted with quick-setting, expansive cement paste. Spacing and length of rock bolts were determined by the quality

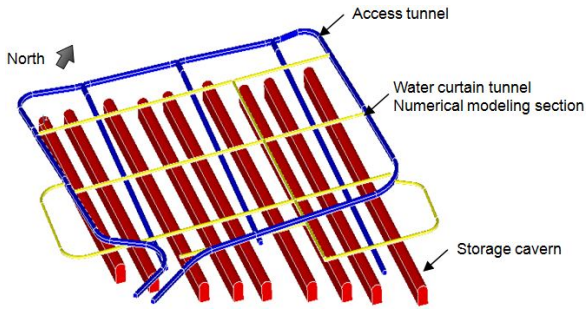

Fig. 1 Underground structures of the crude oil storage facility

of rock mass. Shotcrete (a mixture of cement, aggregates, admixture and water) average depth of 12 cm, varied according to the quality of rock mass.

To prevent groundwater loss from the rock mass and the subsequent groundwater table dropdown, pre- and post-grouting were carried out during the excavation of the storage caverns. During the excavation of the gallery or a bench a 10 m exploratory borehole was drilled before the advance of the working face and the water leakage was measured. If this leakage exceeded the allowable limit of 0.1 liter/min/meter, pre-grouting was carried out 10 m from the working face. Post-grouting was performed at the end of the excavation of the gallery or a bench if a water leakage limit value of 2 liter/day/m^2 was exceeded and the excavation of the next bench was not commenced until this limit was satisfied.

2.2 Engineering geology

The project site is located under a hill with an East-West orientation. Fig. 2 shows the topography and faults around the project area. The average elevation of the hill is about 220 m a.s.l. The buried depth is approximately 120 m. The geology of the study area consists mainly of granite of Cretaceous and Proterozoic, in which the percentage of Proterozoic granite out of all rocks in the project area is about 80. On the basis of cores obtained from drillholes in the area, the dominating rock types are described as granite and aplite. The granite is reddish-grey, medium-to coarse-grained rock with a pronounced gneissic foliation. The aplites are characterized by their fine-grained fabric. Other minor rock types include diorite and amphibolite. The content percentage of minor rocks in mass is less that 10%. Rock mass classification is performed according to Q-system. The system was developed to understand why different Norwegian hydropower caverns displayed widely different deformation magnitudes. The system combined support needs with rock quality and tunnel or cavern span. The Q-value is calculated according to Rock Quality Designation (RQD), joint set numbers, roughness, alteration degree, water inflow effect and strength/stress ratio of rocks. Over 80% of the Q-values belong to fair or very good rock mass type. Generally competent and unweathered rock material provides excellent rock conditions for cavern construction.

At the site, three strike-slip faults were disclosed. The fault F3 is the largest in scale, striking from SW to NE. The dip angle of F3 ranges from 53° to 70°. The thickness of the fault F3 is less 20 m. The strike of the fault F7 is approximately parallel to F3, while that of the fault F8 is NS.

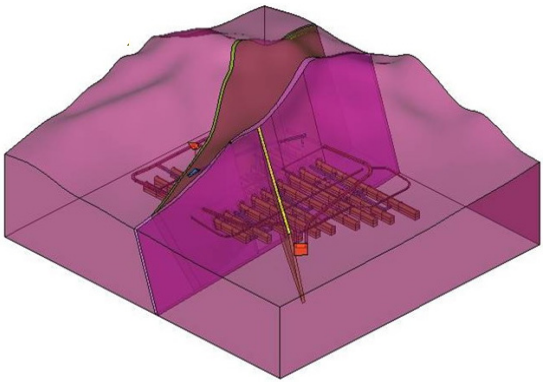

Fig. 2 Topography and faults around the project area (Lv and Li 2016)

The dip angles of both F3 and F8 range from 70 to 80°. Statistical analyses on joint orientation showed that the site could be divided into 5 regions, in which the dominant joint orientations are different. In the five regions, the strikes of dominant joints are NW345° (in region I), NW0° and NE45° and NW300° (in region II), NE45° (in region III), NW0° and NE45~60° and NE30° (in region IV), and NE45~60° and NE30° and NW0° (in region V), respectively. It was also observed that the density of the joints decreases with buried depth in the boreholes.

The in-situ geometrical apertures of joints were measured using a stainless steel feeler gauge, whose measurement capacity ranges from 0.001 mm to 2 mm. The measurement was carried out on the sidewall of the caverns after excavation. 9 hydraulic permeable joints were measured in this study. It was found that the average geometrical aperture of the joints with high inclination angles is 0.02 mm, while that for joints with low inclination angles is about 0.01 mm. To obtain the Joint Roughness Coefficients (JRC) of joints, field measurement and back analysis were performed. In the measurement fresh joint surfaces with a dimension of 300 mm in width and 300 mm in length were mapped using a simple profiler. Three fresh joint surfaces disclosed in cavern #3, #7 and #9 were mapped. From the surfaces, the JRCs of the surface were calculated and range from 3 to 10 using an analytical equation by Barton and Choubey (1977). In the back analysis, the shear stress–shear displacement relations of joints were compared with DEM predictions using different JRCs (Li *et al*. 2014). It was concluded that the average for the JRCs of the joints with high dip angles is about 5.5, while that for joints with low dip angles is about 8.

2.3 Hydrogeology

The groundwater is stored in the form of pore water or fracture water in the project area. The annual precipitation in 20 years averaged 736.2 mm, and heavy rains tend to occur between June and September, in which period over 70% of total precipitation occurs. As the slope of ground surface is steep, the supply from atmospheric precipitation into the rock mass is negligible, with an infiltration coefficient of 0.073. Long-term groundwater level observations have been conducted in 15 drillholes around the caverns in the pre-construction period. It was found that the groundwater level varies with the topography. The groundwater table was 20 m below ground surface in the low part of the site.

2.4 Permeability tests

To obtain reliable estimates of the permeability of the rock mass in the vicinity of the caverns, three different types of test were carried out as follows:

- Thirty (30) groundwater recovery tests in which the water was drained from a borehole and then the relation between the groundwater table in the borehole and the time recorded.
- Seven (7) falling head tests in which a borehole was charged with water and the groundwater table change with time obtained.
- Forty eight (48) groundwater injection tests in which 2 packers were used in a borehole at the similar elevation of the caverns and the pressure in the borehole increased and the groundwater flow rate was measured.

The results of the permeability tests show that the permeability coefficients of the rock mass obtained from groundwater injection tests are higher than those obtained from either the groundwater recovery or the falling head tests, due to the joint opening induced by the injection

pressure. The groundwater recovery and falling head tests were performed in locations near the ground surface. Therefore groundwater recovery and falling head tests may also overestimate the rock mass permeability. For these reasons the value of 1.0×10^{-4} m/d is taken to be representative of the rock mass permeability.

During the construction of the facility, the hydraulic connectivity of the water curtain system was tested. The testing procedures of the water curtain system for the project consisted of three stages: single-borehole water injection test, cross-borehole interconnectivity test and curtain system injection test. The first two tests were used to evaluate the interconnectivity of boreholes in the system. The single-borehole water injection test was employed to obtain the initial hydrostatic pressures in rock mass, whereas cross-borehole interconnectivity test was used to evaluate the interconnectivity of boreholes in the system. The curtain system test was performed to estimate the groundwater inflow rates into the boreholes and the storage caverns. A detailed description on the testing procedure and test results was presented in reference (Wang *et al*. 2015b).

In the single-borehole water injection tests, the permeability coefficients of the rock mass around the boreholes were estimated using the applied water pressure and the measured water flow rate. As a whole, the rock mass in the southeastern area is more permeable than that in the northwestern area. The permeability of the rock mass varies with the location. However, some of the locations of high permeable rock mass were not on or even near the three faults. It should be noted that the permeability coefficients calculated in this manner are the equivalent values of the permeability coefficient tensors. A high equivalent permeability coefficient could be induced by any a component of the permeability tensor, e.g., horizontal or vertical permeability.

3. Estimation using analytical equations

Analytical equations have been derived to estimate the groundwater inflow into underground openings. Four of them were used to estimate the groundwater inflow rate into the facility in this study. Their expressions and assumptions are listed in Table 1 and illustrated in Fig. 3. The physical meanings of the symbols in the equations are as follows:

q: groundwater inflow rate, m^3/d;
k: permeability coefficient of rock mass, m/d;
H_w: groundwater table elevation, m;
r: tunnel radius, m;
s: groundwater table dropdown, m.

In the formulation of all the five equations, it was assumed that (1) the ground is homogeneous and isotropic, with a permeability coefficient of k; (2) the opening is circular in shape with a diameter of r; (3) the flow is in steady state; and (4) the groundwater pressure at the periphery of the opening is zero. However, for Eqs. (1), (2) and (3), the groundwater table above the center of the opening is a constant, while for Eq. (4), the groundwater table drops down after the excavation of the opening.

The estimated groundwater inflow rates using the above analytical equations are also shown in Table 1. In the estimation, the permeability coefficient of the rock mass around the caverns was set to be 1.0×10^{-4} m/d. The estimated flow rates range from 0.0387 to 0.0279 m^3/d. It was found that the inflow rate estimated using the equation by Moon and Fernandez (2010) is lower than those using the other equations, due to the fact that the groundwater dropdown was taken into

Table 1 List of equations for groundwater flow rate estimation

No.	Reference	Equations	Illustration	Estimated groundwater inflow rate
1	(Harr 1962)	$q=\frac{2\pi kH_w}{\ln(2H_w/r)}$		0.0387
2	(El Tani 2003)	$q=2\pi k\frac{\lambda^2-1}{\lambda^2+1}\frac{H_w}{\ln\lambda}$, $\lambda=\frac{H_w}{r}-\sqrt{\left(\frac{H_w}{r}\right)^2-1}$	Fig. 3(a)	0.0386
3	(Park *et al*. 2008)	$q_1=\frac{2\pi k(A+H_w)}{\ln\frac{H_w+\sqrt{H_w{}^2-r^2}}{r}}$, $A=H_w\frac{1-\lambda^2}{1+\lambda^2}$		0.0346
4	(Moon and Fernandez 2010)	$q_1=\frac{2\pi k(H_{w0}-s)}{\ln(2H_w/r)}$	Fig. 3(b)	0.0279

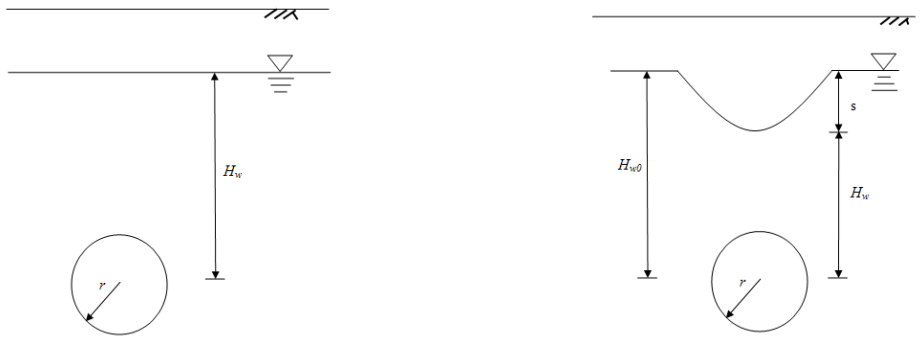

(a) (b)

Fig. 3 Illustration of the boundary conditions and assumptions for the equations in Table 1

consideration in the derivation of the equation. However, the estimated inflow rates into different caverns using any one of the analytical equations would be more or less the same, as the analytical equations do not consider the influences of neighboring caverns on groundwater flow rate.

4. Numerical modeling

4.1 Finite element method

The length of the caverns is much greater than the cross section dimensions so that the plane strain condition was assumed in this study. The horizontal extent of the cross section used for the

study is 2530 m and its base at El (-350) m is 300 m below the cavern floor. This section locates at the place where a water curtain tunnel was placed as shown in Fig. 1. The mesh consists of 5807, 8-node biquatratic reduced integration plain strain hybrid elements with linear pressure.

The stress-displacement boundary conditions are as follows. In the plain strain analysis the coordinate system will be X-Y, X being the horizontal, and Y the vertical direction respectively. The displacement boundary conditions will be the follows: horizontal displacement, $u_x = 0$, on the two vertical sides of the model and the two displacements, $u_x = u_y = 0$, on the base of the model. The top surface is stress free and has no displacement constraints. The excavation of the caverns is simulated by releasing nodal forces on the cavern peripheries.

The boundary conditions for fluid flow were assumed as follows. The effects of crude oil storage and the water curtain pressures generate surface pressure on the cavern peripheries and water tunnel peripheries, respectively. The fluid flow boundary conditions allow no flow from the ground surface. The groundwater pressures vary with the buried depth of nodes on the outer sides (vertical and base) of the model. The initial geo-stresses and groundwater pressures vary in accordance with the in-situ measurements and these effects were modelled using the ABAQUS subroutines, SIGNI and UPOREP (ABAQUS Inc. 2006).

The Drucker-Prager (DP) material failure hypothesis was used to model the rock, which is a frictional material with failure depending on the mean compression stress and with compression strength much greater than its tensile strength. A back analysis on the material parameters were performed (Wang *et al*. 2011). The material properties used in the analyses are given in Table 2.

In this study, the permeability coefficient of the rock mass around the caverns was set to be 1.0×10^{-4} m/d, which is representative of the rock mass permeability according to the permeability tests.

The estimation on groundwater inflow into the caverns is shown in Fig. 4. The estimated groundwater pressure distribution around the facility is shown in Fig. 5. The groundwater inflow

Table 2 Mechanical parameters for rock mass used in FEM analysis

Property	Dry density	Porosity	Young's modulus	Poisson's ratio	Friction angle	Dilation angel	Cohension
Value	2780 Kg/m^3	0.005	21 GPa	0.21	32°	20°	8.3 MPa

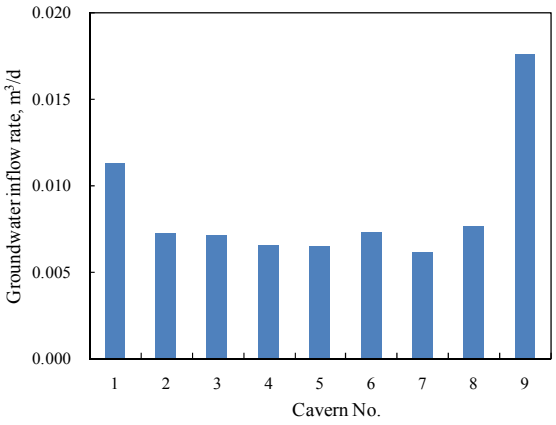

Fig. 4 Groundwater inflow rates into the caverns estimated using FEM modeling

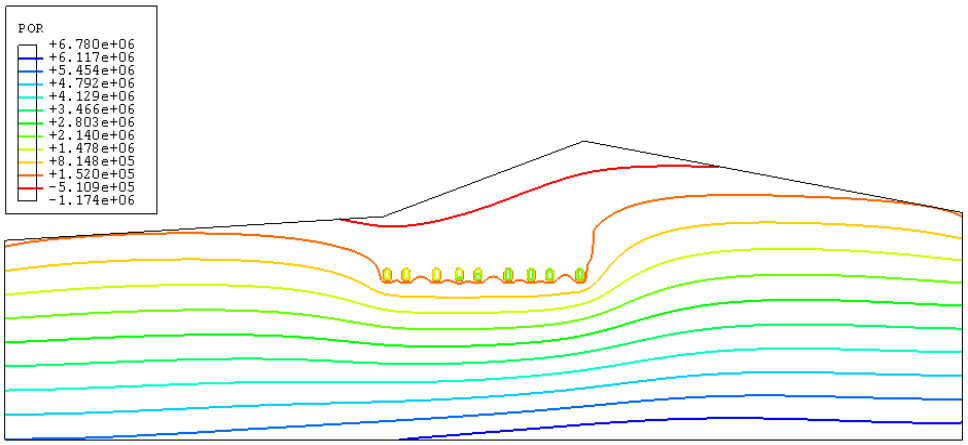

Fig. 5 Groundwater pressure distribution around the caverns estimated using FEM modeling showing that the hydraulic gradients on the left side of cavern No. 1 and on the right side of cavern No. 9 are higher than those at the other caverns (unit: Pa) (from left to right, caverns no. 1 to no. 9)

rate into cavern No. 9 is the highest, with a value of 0.0176 m^3/d, and that into cavern No. 7 is the lowest, with a value of 0.0064 m^3/d, among the 9 caverns. The average groundwater inflow rate is about 0.0086 m^3/d. It is also shown that the groundwater inflow rate into cavern No. 1 is also higher, compared to those at the caverns from No. 2 to No. 8. The high groundwater inflow rates at caverns No. 1 and 9 than those at other caverns are induced by the fact that hydraulic gradients on left side of cavern No. 1 and on the right side of cavern No. 9 are much higher than those around the other caverns, as shown in Fig. 4. The presence of neighbouring caverns reduces the hydraulic gradients around the caverns from No. 2 to No. 8.

A parameter sensitivity analysis showed that the groundwater inflow rate is a power function of the permeability coefficient of rock mass (Wang *et al*. 2013). The value of the power in the function is about 0.67, which is different from that in analytical equations, i.e., 1. It is indicated that the groundwater inflow rate would be overestimated using analytical equations, which do not consider the influence of neighboring caverns.

As what was shown in the permeability tests, the permeability coefficient varies with the locations of the tests. A more detailed numerical model with the variation of permeability coefficient with the locations of rock mass would improve the prediction accuracy. However, more permeability tests would be required in order to establish the detailed numerical model.

4.2 Discrete element method

To estimate the groundwater inflow into the underground crude oil storage facility, a 2D discrete element model is constructed using a code UDEC (Itasca Inc. 2000). The model is perpendicular to the cavern axis, and the geological and hydrogeological conditions in the area are typical for the site. The area is 800 m wide and 350 m high. The horizontal distances from caverns to outer boundaries of the model is 130 m, while the vertical distances from caverns to model bottom boundary is 80 m. This section is identical to that in FEM. To be noted, the area of the UDEC model was smaller than that of the FEM model because the solving of hydro-mechanical coupling problem using DEM requires much more computation capacity than that using FEM.

Table 3 Geometrical parameters of joints for DEM analysis

No.	Concentration (counts/m)	Apparent dip angles (°)		Trace length (m)		Depth (m)	
		mean	Standard variance	mean	Standard variance	Left boundary	Right boundary
1	0.16	76	6.2	23.2	5.8	0~200	220~300
	0.11	24	27	26.8	6.3		
2	0.3	76	5	18.7	4.7	0	0~220
	0.14	24	27	21.2	5.4		
3	0.16	76	5	28.3	7.6	80~300	80~380
	0.11	24	27	31.2	8.2		
4	0.3	76	5	24.7	5.3	0~80	0~80
	0.15	24	27	26.9	6.1		

According to field investigations on joint distribution, the density of joints in the rock mass depends on the buried depth. In the simulation, the area of study is divided into four domains, in which the geometrical parameters of joints are different. Table 3 presents the geometrical parameters for the joints in the domains. In principle, two sets of joints were observed in this region. The average dip angle of one set is 24°, while the average dip angle of the other is 76°. The density of joints in domains #1 and #3 are lower than those in domains #2 and #4, because the field investigations indicate that the density of joints decrease with buried depth in site. The trace lengths of the joints were estimated using the measures of the outcrop on ground surface and excavation faces.

The boundary conditions were prescribed as follows. No vertical displacements were allowed along the base of the meshes. No lateral displacements were allowed along the vertical side of the meshes. The top surface of the meshes was allowed to deform freely. No fluid flow was allowed at the base of the meshes. The hydrostatic fluid pressure was applied at the left and right boundary.

Barton-Bandis joint model (Barton *et al*. 1985) was adopted in the analysis. The principle of the hydro-mechanical coupling effect was described in (ABAQUS Inc 2000, Li *et al*. 2014). The hydro-mechanical parameters are presented in Table 4. The parameters for shear deformation and strength are obtained from the back analysis using the direct shear test results (Li *et al*. 2014).

The hydraulic conductivity of jointed rock mass is sensitive to aperture change based on the cubic law (Witherspoon *et al*. 1980). Flow in planar rock joints may be idealized by means of the parallel plate model, and the analytic solution for laminar viscous flow between parallel plates gives the fluid rate (Itasca Inc. 2000). As the hydraulic aperture can vary under various conditions, it is difficult to measure the hydraulic aperture. The joint samples prepared by splitting could not

Table 4 Mechanical parameters for rock mass used in DEM analysis

Parameter	Shear stiffness	Normal stiffness	Residual friction angle	Lab-scale roughness coefficient	Lab-scale wall compression strength	Lab-scale joint length	Residual aperture	Initial aperture
Joint set #1	10 GPa/m	3 GPa/m	20°	5.5	60 MPa	0.2 m	0.01 mm	0.02 mm
Joint set #2	10 GPa/m	3 GPa/m	17°	8	60 MPa	0.2 m	0.01 mm	0.02 mm

represent normal deformation behavior of the joints in the field situation. The hydraulic aperture in this study is evaluated using a case study (Li *et al*. 2014).

Fig. 6 shows the groundwater flow rates into the caverns with the water curtain pressures of 30 kPa. The groundwater flow rates for the caverns range from -0.0007 to 0.0411 m^3/d per meter of cavern. The average groundwater flow rate is about 0.0164 m^3/d per meter of cavern. The rates are high at the caverns No. 2, 4, 6 and 7. Fig. 7 shows the groundwater pressure distribution around the caverns. In the figure, dense lines represent high pressure. It was found that the high groundwater inflow rates in caverns No. 2, 4, 6 and 7 are induced by the appearance of the high permeable joints with high pressures around the caverns, especially under the cavern floors. Hence, the estimation on the spatial distribution of groundwater inflow using DEM depends greatly on the distribution of joints and their permeable properties, such as the apertures and connectivity of joints in different locations.

To be noted, the groundwater inflow rate into caverns #1 is negative. This could be induced by the shear dilation of rock joints around the caverns. Within the shear dilating zone, the hydraulic gradients will direct from the cavern to rock mass. The groundwater would flow from the cavern to the rock mass according to the parallel plate model.

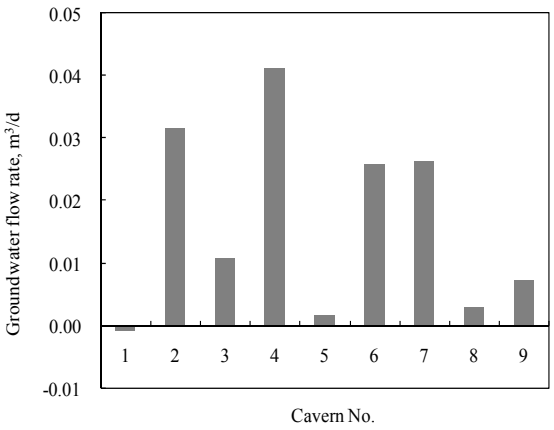

Fig. 6 Groundwater inflow rates into the caverns estimated using DEM modeling

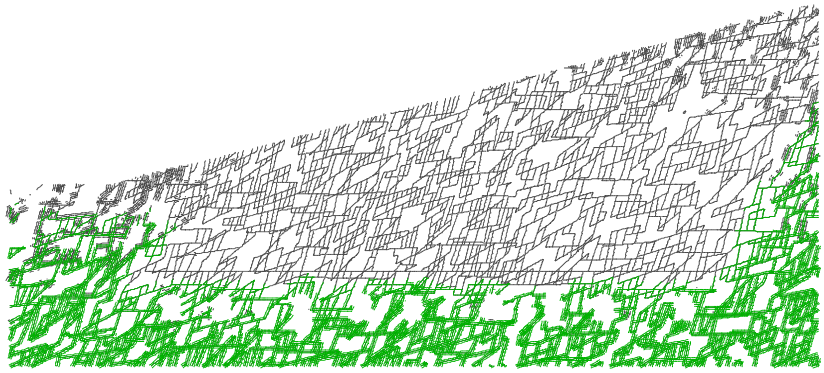

Fig. 7 Groundwater pressure distribution in the study area estimated using DEM modeling (from left to right, caverns no. 1 to no. 9; Dense lines represent high pressure)

5. Field measurement

5.1 Measurement method

The measurement was performed for the 9 storage caverns. The groundwater inflows at leakage spots were collected using a plastic sheet. The groundwater inflow volume in half an hour was measured for each spot using a graduated flask. The inflow rate was calculated by dividing the volume with the period of time, i.e., half an hour. In the measurement, the groundwater inflow was collected as much as possible. However, groundwater inflow at the leakage spots on the floors of the caverns could be missed as the floors were covered by gravels at the moments of measurement.

In the measurement, the leakage spots were divided into three types.

- Point leakage (see Fig. 8(a)). Point leakage occurs at single points at which rock joints were intersected. This type of leakage occurs at the rock mass of good quality.
- Line leakage (see Fig. 8(b)): Line leakage occurs along one joint with more than 1 leakage point. This type of leakage usually occurs at the rock mass with only 1 dominant permeable rock joint.
- Surface leakage (see Fig. 8(c)). Surface leakage occurs along several joints with a number of leakage points. This type of leakage occurs at the rock mass of poor quality and with several dominant permeable rock joints.

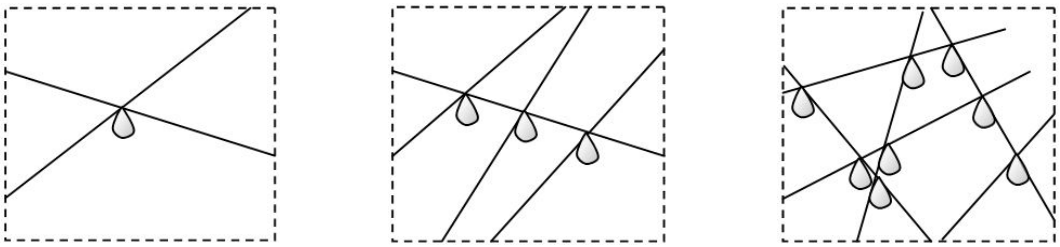

(a) Point leakage (b) Line leakage (c) Surface leakage

Fig. 8 Types of leakage spots around cavern periphery

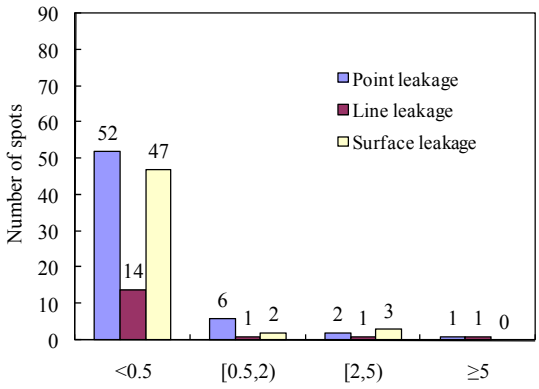

Fig. 9 Numbers of leakage spots in terms of the magnitudes of inflow rate (unit: L/min)

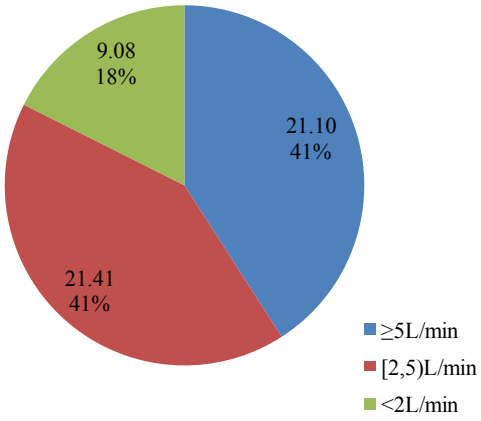

Fig. 10 Total groundwater flow rates with different magnitudes of inflow rate (Unit: L/min)

5.2 Measured results

In the measurement, no visual leakage spots were observed in the caverns No. 3 and 5. There were 61, 17 and 54 leakage spots of the point, line and surface leakage types, respectively. The total groundwater inflow rates of the point, line and surface leakage spots are 21.3, 11.2 and 19.1 L/min, respectively.

Fig. 9 compares the numbers of the leakage spots with different ranges of groundwater inflow rate. The number of the leakage spots with high groundwater inflow rates is few, e.g., the number for the spots with an inflow rate not less than 2 L/min is 8. Fig. 10 compares the total groundwater inflow rates of the spots with different range of rates. The total groundwater inflow rate of the 8 spots is about 42 m^3/d. The percentage of the inflow rate of the two spots among the total inflow rate is about 82. Therefore, the several high rate spots contribute greatly to the total rate for the 9 caverns. The spatial distribution of groundwater inflow rates is nonuniform. It is indicated that the permeable property of the rock mass is highly nonhomogeneous.

The locations of the spots are shown on Fig. 11, along with their magnitudes of inflow rates. The size of the symbols represents the magnitude of the inflow rates. Most of the leakage spots locate on the trace of faults. It is also shown that some spots are closely related to the permeable curtain boreholes, e.g., the spots on the south part of caverns No. 1 and 9. However, in some area, there are not many leakage spots with high inflow rate in field measurement in caverns although in curtain injections tests, the permeability of rock mass is high. This could be explained as that the rock mass has a higher permeability component in horizontal direction than that in vertical direction.

Fig. 12 compares the groundwater inflow rates into the caverns. The rates into the caverns No. 1, 5, 7 and 9 are high, while those into the other caverns are low. The spatial distribution of groundwater inflows among the caverns are different from those estimated by both FEM and DEM. The total groundwater inflow rate into the 9 caverns is about 51.6 m^3/d, which is consistent with those estimated using both FEM and DEM. Detailed discussions on the estimation of the magnitude and spatial distribution of groundwater inflow rate are presented in the next section.

A careful field investigation was performed on the 8 major leakage spots with groundwater inflow rates not less than 2 L/min. It was found:

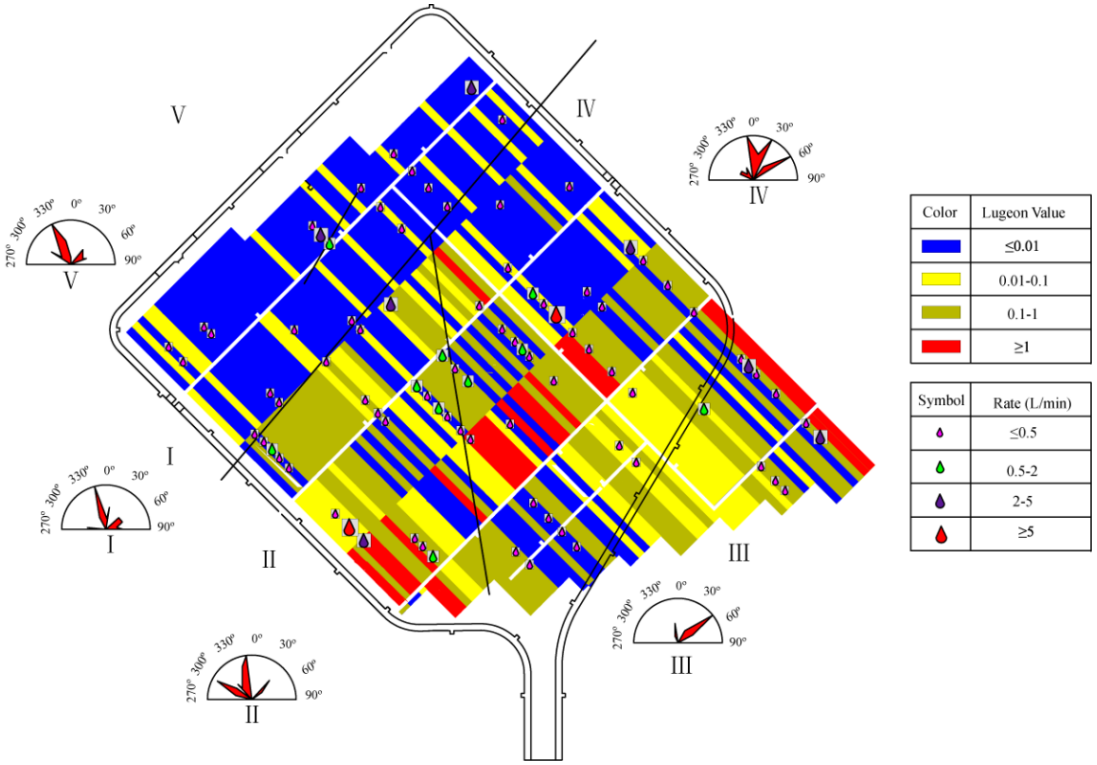

Fig. 11 The magnitude and distribution of groundwater inflow into caverns in context of the distribution of rock mass permeability coefficients obtained in single borehole injection test, and the locations of main faults and dominant rock joint orientations obtained in geological investigation

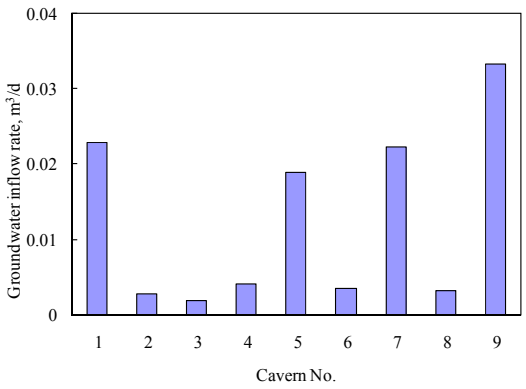

Fig. 12 Groundwater flow rates into different caverns in field measurement

- Permeable joints, fractured zone or dykes were developed in the rock mass;
- Some of the joints were filled with altered minerals;
- The joints were induced by shear and/or tensile tectonic stress.

These findings are consistent with those by Zarei *et al*. (2011)

6. Discussions

6.1 Groundwater inflow rate

Fig. 13 compares the groundwater inflow rates into the facility estimated using analytical equations, FEM modeling, DEM modeling and field measurement. It is shown that the estimations using analytical equations are much higher than those using FEM, DEM and field measurement, while the estimations using both FEM and DEM are consistent with that in field measurement. The high magnitude of groundwater inflow rate estimated using analytical equations could be induced by the assumptions on the constant groundwater table and/or no consideration on the influence of neighbouring openings. However, because in FEM and DEM modeling the assumptions are removed, the estimated magnitudes of groundwater inflow rate into the facility are consistent with each other and with that in field measurement.

From the comparison of the estimations, it would be concluded that both FEM and DEM would give good estimations on groundwater inflow rate into the facility when the hydro-mechanical properties of the rock mass, the initial and/or boundary conditions and the analysis procedures are properly prescribed in numerical modeling.

In addition, on one hand, as the estimation by FEM is close to that by field measurement, the size of (Representative Element Volume) REV for the rock mass is smaller than that of the facility; on the other hand, as the groundwater inflow rates at different caverns are different, the size of REV is higher than that of single caverns.

6.2 Spatial distribution of groundwater inflow

The spatial distribution of groundwater inflow is important for distribution of pumping capacity and the design of the grouting work. If the spatial distribution could be estimated, an efficient pump distribution and grouting strategy would be raised. In this study, the field measurement showed that several high rate leakage spots contributed more than half of the inflow rate into the facility. Fig. 11 shows the locations of leakage spots, along with the locations of faults and the Lugeon values of rock mass around boreholes in single borehole injection tests. The locations of

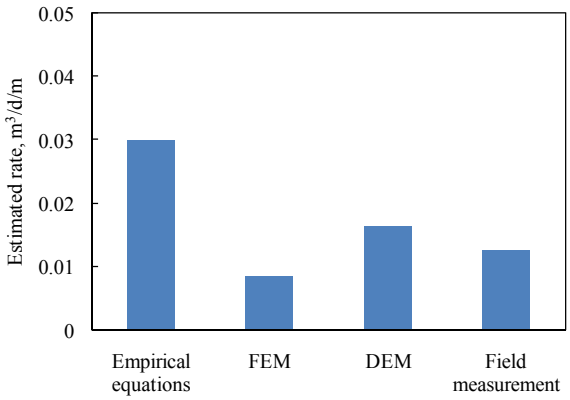

Fig. 13 Groundwater inflow rates per meter estimated using various methods (the value of empirical equations is subject to change using different expressions)

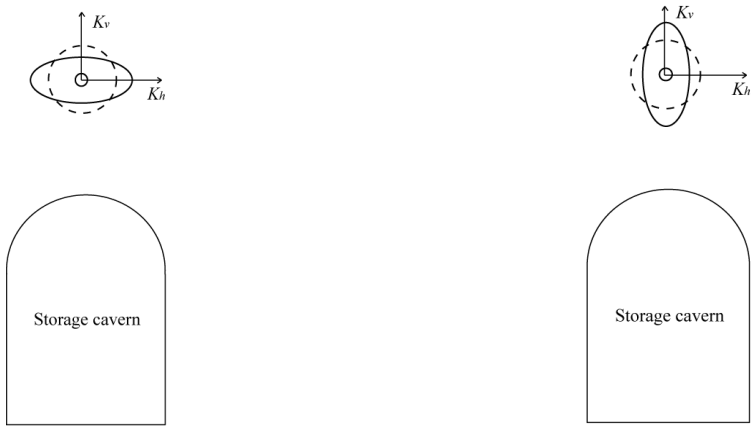

(a) $K_h > K_v$ (b) $K_v > K_h$

Fig. 14 Illustration on the effects of relation of permeability components on the measured groundwater inflow rates for two boreholes with identical Lugeon value in single borehole injection tests

these leakage spots are closely related to the locations of faults and high permeable curtain boreholes. However, in the denoted area (in the white ellipse), the rock mass has a higher permeability in curtain injections tests while there are not many spots with high inflow rate in field measurement in caverns. This phenomenon could be attributed to a high horizontal permeability component but a low vertical component for the rock mass. Fig. 14 illustrates the effects of the relation of permeability components on the measured groundwater inflow rates for two boreholes with identical Lugeon values. In the figure, the solid circles denote the permeability tensor in 2D space, while the dashed circle represents the measured permeability from the borehole injection tests. In Fig. 14(a) the horizontal component is higher than the vertical component of permeability, which will lead to a higher inflow rate, and thereby more inflow spots, than in the situation shown in Fig. 14(b), i.e., the vertical component is higher than horizontal component of permeability.

In this study, the spatial distributions of groundwater inflow estimated by both FEM and DEM are nonuniform. However, the spatial distribution observed in field measurement was not successfully predicted using neither FEM nor DEM on this stage. A more detailed FEM or DEM numerical model would improve the accuracy on the spatial distribution estimation of groundwater inflow. Nevertheless, the permeable property of rock mass should be characterized in an acceptable accuracy. Specifically, the property is the permeability coefficient variation with location for FEM modeling, while it is the distributions of joint orientation and aperture for DEM modeling.

7. Conclusions

Groundwater inflow into a pilot underground storage facility in China was estimated using analytical equations, numerical modeling and field measurement. The measured and predicted magnitude and spatial distribution of groundwater flow rate were compared. The implications from the comparison of the estimation methods were presented. The applicability of numerical modeling and the role of rock mass characterization in the estimation of groundwater inflow were discussed. The concluding remarks are summarized as follows.

(1) Characterization of hydro-mechanical properties of rock mass plays a critical role in estimating the groundwater inflows into underground facilities;
(2) The magnitude of groundwater inflow rate could be estimated with a higher accuracy by both FEM and DEM than those by analytical equations, due to the fact that in analytical equations simplified assumptions were adopted;
(3) The spatial distribution of groundwater inflow is highly non-uniform, and is closely related to the locations of faults and high permeable curtain boreholes in global scale; and
(4) A more detailed FEM or DEM numerical model would improve the accuracy on the spatial distribution estimation of groundwater inflow. Nevertheless, the permeable property of rock mass should be characterized in an acceptable accuracy.

Acknowledgments

This study was financially supported by the National Natural Science Foundation of China under contract Nos. 51579141, 51309145, and 5151101078, and by State Key Laboratory for Geomechanics and Deep Underground Engineering, China University of Mining & Technology under contract No. SKLGDUEK1408.

References

ABAQUS Inc. (2006), ABAQUS manual, Version 6.6.

Barton, N. and Choubey, V. (1977), "The shear strength of rock joints in theory and practice", *Rock Mech*., **10**(1), 1-54

Barton, N., Bandis, S. and Bakhtar, K. (1985), "Strength, deformation and conductivity coupling of rock joints", *Int. J. Rock Mech. Min. Sci. & Geomech. Abs*., **22**(3), 121-140.

Cesano, D., Olofsson, B. and Bagtzoglou, A.C. (2000), "Parameters regulating groundwater inflows into hard rock tunnels – a statistical study of the Bolmen tunnel in Southern Sweden", *Tunn. Undergr. Sp. Tech*., **15**(2), 153-165.

Cesano, D., Bagtzoglou, A.C. and Olofsson, B. (2003), "Quantifying fractured rock hydraulic heterogeneity and groundwater inflow prediction in underground excavations: The heterogeneity index", *Tunn. Undergr. Sp. Tech*., **18**(1), 19-34.

Coli, N., Pranzini, G., Alfi, A. and Boerio, V. (2008), "Evaluation of rock-mass permeability tensor and prediction of tunnel inflows by means of geostructural surveys and finite element seepage analysis", *Eng. Geo*., **101**(3), 174-184.

El Tani, M. (2003), "Circular tunnel in a semi-infinite aquifer", *Tunn. Undergr. Sp. Tech*., **18**(1), 49-55.

Fernandez, G. and Moon, J. (2010a), "Excavation-induced hydraulic conductivity reduction around a tunnel – Part 1: Guideline for estimate of ground water inflow rate", *Tunn. Undergr. Sp. Tech*., **25**(5), 560-566.

Fernandez, G. and Moon, J. (2010b), "Excavation-induced hydraulic conductivity reduction around a tunnel – Part 2: Verification of proposed method using numerical modeling", *Tunn. Undergr. Sp. Tech*., **25**(5), 567-574.

Harr, M.E. (1962), *Groundwater and Seepage*, Dover Publications, New York, NY, USA.

Harrison, J.P. and Hudson, J.A. (2000), *Engineering rock mechanics. Part 2*: *Illustrative workable examples*, Pergamon, Oxford, UK.

Itasca Inc. (2000), Universal Distinct Element Code User's Guide, Version 3.1, Minneapolis, MN, USA.

Jing, L. (2003), "A review of techniques, advances and outstanding issues in numerical modelling for rock mechanics and rock engineering", *Int. J. Rock Mech. Min. Sci*., **40**(3), 283-353.

Kolymbas, D. and Wagner, P. (2007), "Groundwater ingress to tunnels – The exact analytical solution",

Tunn. Undergr. Sp. Tech., **22**(1), 23-27.
Li, S., Wang, Z., Ping, Y., Zhou, Y. and Zhang, L. (2014), "Discrete element analysis of hydro-mechanical behavior of a pilot underground crude oil storage facility in granite in China", *Tun. Undergr. Sp. Tech.*, **40**, 75-84.
Liu, R., Jiang, Y., Li, B. and Wang, X. (2015), "A fractal model for characterizing fluid flow in fractured rock masses based on randomly distributed rock fracture networks", *Comput. Geotech.*, **65**, 45-55.
Liu, R., Li, B., Jiang, Y. and Huang, N. (2016a), "Review: Mathematical expressions for estimating equivalent permeability of rock fracture networks", *Hydrogeo. J.*, **24**(7), 1623-1649.
Liu, R., Yu, L. and Jiang, Y. (2016b), "Fractal analysis of directional permeability of gas shale fracture networks: A numerical study", *J. Nat. Gas Sci. Eng.*, **33**, 1330-1341.
Liu, R., Li, B. and Jiang, Y. (2016c), "A fractal model based on a new governing equation of fluid flow in fractures for characterizing hydraulic properties of rock fracture networks", *Compu. Geotech.*, **75**, 57-68.
Lv, B. and Li, Y. (2016), *Integrated Innovations of Key Technology for Construction of Large-Scale Crude-Oil Reserve Underground Water-Curtaining Caverns Project*, China Petrochemical Press, Beijing, China.
Marechal, J-C., Lanini, S., Aunay, B. and Perrochet, P. (2014), "Analytical solution for modeling discharge into a tunnel drilled in a heterogeneous unconfined aquifer", *Groundwater*, **52**(4), 597-605.
Mas Ivars, D. (2006), "Water inflow into excavations in fractured rock – A three-dimensional hydro-mechanical numerical study", *Int. J. Rock Mech. Min. Sci.*, **43**(5), 705-725.
Molinero, J., Samper, J. and Juanes, R. (2002), "Numerical modeling of the transient hydrogeological response produced by tunnel construction in fractured bedrocks", *Eng. Geo.*, **64**(4), 369-386.
Moon, J. and Fernandez, G. (2010), "Effect of excavation-induced groundwater level drawdown on tunnel inflow in a jointed rock mass", *Eng. Geo.*, **110**(3), 33-42.
Park, K., Owatsiriwong, A. and Lee, J. (2008), "Analytical solution for steady-state groundwater inflow into a drained circular tunnel in a semi-infinite aquifer: A revisit", *Tunn. Undergr. Sp. Tech.*, **23**(2), 206-209.
Perello, P., Baietto, A., Burger, U. and Skuk, S. (2014), "Excavation of the Aica-Mules pilot tunnel for the Brenner base tunnel: Information gained on water inflows in tunnels in granitic massifs", *Rock Mech. Rock Eng.*, **47**(3), 1049-1071.
Perrochet, P. and Dematteis, A. (2007), "Modeling transient discharge into a tunnel drilled in a heterogeneous formation", *Ground Water*, **45**(6), 786-790.
Wang, Z., Li, S., Lv, X. and Xue, Y. (2011), "Parameter sensitivity of rock mass integrity for a pilot underground crude oil storage caverns during construction phase", *Rock Soil Mech.*, **32**(2), 488-495. [In Chinese]
Wang, Z., Li, S., Qiao, L., Ping, Y., Zhang, L. and Jiang, Y. (2013), "Assessment of natural containment properties of an underground crude oil storage cavern using fluid flow-stress coupling method", *Chin. J. Geotech. Eng.*, **35**(8), 1535-1543. [In Chinese]
Wang, Z., Li, S., Qiao, L. and Zhang, Q. (2015a), "Finite element analysis of the hydro-mechanical behavior of an underground crude oil storage facility in granite subject to cyclic loading during operation", *Int. J. Rock Mech. Min. Sci.*, **73**, 70-81.
Wang, Z., Li, S. and Qiao, L. (2015b), "Assessment of hydro-mechanical behavior of a granite rock mass for a pilot underground crude oil storage facility in China", *Rock Mech. Rock Eng.*, **48**(6), 2459-2472.
Wang, Z., Li, S. and Qiao, L. (2015c), "Design and test aspects of the water curtain system for a pilot underground oil storage caverns in China", *Tunn. Undergr. Sp. Tech.*, **48**, 20-34.
Witherspoon, P.A., Wang, J.S.Y., Iawi, K. and Gale, J.E. (1980), "Validity of cubic law for fluid flow in a deformable rock fracture", *Water Res. Res.*, **16**(6), 1016-1024.
Zarei, H.R., Uromeihy, A. and Sharifzadeh, M. (2011), "Evaluation of high local groundwater inflow to a rock tunnel by characterization of geological features", *Tunn. Undergr. Sp. Tech.*, **26**(2), 364-373.